



ELSEVIER

Physica D 135 (2000) 212–232

PHYSICA D

www.elsevier.com/locate/physd

Being stable and discrete

N.J. Balmforth^a, R.V. Craster^{b,*}, P.G. Kevrekidis^c

^a *Instituto di Cosmogeofisica, C. Fiume 4, 10133 Torino, Italy*

^b *Department of Mathematics, Imperial College of Science, Technology and Medicine, London SW7 2BZ, UK*

^c *Department of Physics and Astronomy, Rutgers University, Piscataway, NJ 08855-0849, USA*

Received 16 February 1999; received in revised form 14 May 1999; accepted 21 May 1999

Communicated by C.K.R.T. Jones

Abstract

Many discrete lattice systems possess solutions that take the form of localized, stationary structures. In this communication we introduce the discrete version of the Evans function, an analytic function whose zeros correspond to the eigenvalues of the linear stability problem for a spatially localized equilibrium solution. This function provides a convenient and useful tool for investigating the linear eigenvalue spectrum. Notably, it allows us to construct sufficient stability conditions and detect “internal modes” (neutral oscillatory modes that correspond to localized oscillations about the static structure). We illustrate with the discrete sine-Gordon equation, also known as the Frenkel–Kontorova model. A complementary approach suitable for systems with nearest neighbour coupling and based upon techniques of linear algebra (the bisection method) is also described. ©2000 Elsevier Science B.V. All rights reserved.

PACS: 63.20.P; 46.10

Keywords: Discretization; Sine-Gordon equation; Evans function; Localized objects

1. Introduction

A rapidly increasing number of papers over the last 15 years (commencing with the work of Peyrard and Kruskal in 1984 [1]) have demonstrated significant differences in the behaviour of the partial differential equations of continuum nonlinear field theories (such as the sine-Gordon, or the nonlinear Schrödinger models) and their spatially discrete relatives. The discretization of these equations (usually involving the replacement of second spatial derivatives with differences by means of three-point stencils) brings about a number of critically important modifications to the dynamics. Notably, the discretization destroys the translational invariance of the system and, in many cases, precludes the existence of steadily propagating solutions. Instead, the moving kinks and solitary waves of the continuum theories become propagating structures that decelerate by shedding “radiation” (unlocalized wave-like

* Corresponding author.

E-mail address: craster@ma.ic.ac.uk (R.V. Craster)

disturbances) as they traverse the lattice sites. This ultimately brakes the structures and brings them to rest, or “pins” them [1–5]. Thus, rather than the familiar interactions and dynamics of moving coherent structures, the analysis of lattice systems often focusses on stationary, localized objects.

A similar phenomenon occurs for discrete models of reaction–diffusion systems [6]. Here, propagation ceases when the elements of the system lose their interconnectivity (at weak coupling strength). This “propagation failure” has potentially important applications for excitable neurological systems [7,8], in chemical reactions [9] and optics [10]. Notably, the failure of propagation in these systems is associated with the existence of stationary front solutions at low coupling strength. Conversely one can view the emergence of propagating structures as resulting from the disappearance of such stationary solutions as one increases the coupling.

A useful technique in the study of spatially localized structures is a method that we attribute to Evans [11]. Basically, the method allows us to predict if such a structure is linearly stable, and, if not, enables us to detect what kinds of instabilities the equilibrium may suffer. In the continuum theories this method involves the construction of a function, the Evans function, from a differential eigenvalue problem. This function contains detailed information regarding the linear eigenspectrum of the stability problem for coherent structures. It was originally introduced by Evans to study the stability of impulses in continuum nerve axon models, but has lately been implemented in the stability analysis of travelling waves or pulse solutions in a variety of other continuum models [12–15]. More specifically, according to several rigorously proved theorems [12,16], the zeros of this function correspond to the discrete unstable eigenvalues of the coherent structures under study.

Our goal in the present work is to adapt the Evans function to discrete systems. As we shall show for lattices, the construction of the Evans function is even more straightforward than in the corresponding continuum problems. However, our formulation is restricted to studying the stability of stationary equilibria. The reason for this is connected to the lack of translational invariance, and the difficulty in finding travelling wave solutions (these satisfy advance–delay difference equations [6]).

To illustrate, we consider the discrete version of the sine-Gordon equation, also known as the Frenkel–Kontorova model [17]. This equation describes evolution of the displacements, $y_n(t)$, of the elements of a lattice, and can be written in the form,

$$\ddot{y}_n = (y_{n+1} + y_{n-1} - 2y_n) - \frac{1}{d^2} \sin y_n, \quad (1)$$

where the subscripts $n - 1$, n and $n \pm 1$ denote successive lattice sites and d is a parameter measuring the degree of discreteness (small d implies large discreteness and as $d \rightarrow \infty$ we recover the continuous sine-Gordon system). The equation also describes a lattice of coupled pendula.

This model has a variety of stationary kink solutions [1] (see also Section 2). In this instance, although the Evans functions are of limited usefulness for ascertaining the stability of the kinks, they are helpful in uncovering several other features of the linear eigenspectrum (see Section 3). In particular, we can detect “internal” or “shape modes”, spatially localized oscillations about the kink equilibrium [18,19]; these kinds of oscillations are important in understanding kink dynamics and pinning. In addition, along the way, we uncover some interesting properties of a certain class of kinks (Peyrard and Kruskal’s 4π -kinks).

We also connect the Evans function method with a technique from linear algebra; this is the bisection method which works for tridiagonal matrix systems [20,21]. This is the form that the stability problem takes for discrete systems with nearest neighbour coupling, such as the discrete sine-Gordon. Although the matrix methods are formally finite dimensional we can adapt them for the infinite dimensional problem we face in Section 4. A simple connection with Evans functions emerges, and this simplifies the stability theory even further for systems like discrete sine-Gordon.

2. Tracing equilibria from the uncoupled limit

The stationary kink equilibria, $y_n(t) = Y_n$, satisfy

$$0 = Y_{n+1} + Y_{n-1} - 2Y_n - \frac{1}{d^2} \sin Y_n, \quad (2)$$

with $Y_n \rightarrow \text{constant}$ as $n \rightarrow \pm\infty$. In general, we cannot solve this equation in closed form, and we turn to numerical techniques. These techniques are based on Newton iteration; we focus on a lattice of finite size, and apply boundary conditions based on the form of the exponentially decaying tails of localized kinks. To begin the iteration we could choose the continuum sine-Gordon kink, but this proves not to be very efficient at lower coupling strengths and misses many of the equilibria of the problem. Instead, we trace equilibria from the uncoupled limit: $d = 0$.

At $d = 0$ we replace Eq. (1) by

$$\sin Y_n = 0. \quad (3)$$

From here, we read off the equilibria of the pendulum: $Y_n = \pi m$, $m = 0, 1, 2, \dots$. Moreover, we know that the solutions with m even are stable, and those with odd m are unstable.

Now we couple the systems back together. For sufficiently small d , the equilibria existing at $d = 0$ remain in existence; moreover, they also remain stable or unstable according to their uncoupled stability (this can be proved using the implicit function theorem in some appropriate function space; see [10,23]). The goal is now to exploit this property of the system, and build solutions for finite d from the uncoupled equilibria [24].

Evidently, any combination $Y_n = \pi m$ is a solution of the uncoupled problem. Those that look like fronts have $Y_n = 0$ off to the left, and $Y_n = 2M\pi$ off to the right (we restrict the rightward asymptote to be an even multiple of π for obvious reasons of stability).

For 2π -kinks we may take either

$$Y_n = \begin{cases} 0, & \text{for } n < 0, \\ 2\pi, & \text{for } n \geq 0, \end{cases} \quad \text{or} \quad Y_n = \begin{cases} 0, & \text{for } n < 0, \\ \pi, & \text{for } n = 0, \\ 2\pi, & \text{for } n > 0. \end{cases} \quad (4)$$

If we continue these solutions to finite d , we will generate two 2π -kinks. Results of this procedure are shown in Fig. 1 which displays the kink energies $d^{-2} \sum_n \cos Y_n$ against d . The first kink is off-centred in the sense that the displacements at its two central lattice points straddle π . Since this structure is stable at $d = 0$, we expect that it remains so for finite coupling. The second is a centred kink and unstable at $d = 0$. As d increases, the energies of the kinks becomes similar and the solutions converge to the form of the continuum sine-Gordon kink. Based on the fact that the off-centred kink has lower energy, one expects that this kink remains stable at higher d , and the centred kink continues to be unstable; the energy difference is the ‘‘Peierls–Nabarro’’ energy (a term coined from the theory of dislocations, wherein it corresponds to the amount of energy required for a dislocation to move by one site on the lattice) [1]. Nonetheless, the presence of this energy barrier separating the two equilibria does not establish stability or instability, which motivates the analysis of Section 3.

For 4π -kinks, we may again do a similar construction. From

$$Y_n = \begin{cases} 0, & \text{for } n < 0, \\ 4\pi, & \text{for } n \geq 0, \end{cases} \quad \text{or} \quad Y_n = \begin{cases} 0, & \text{for } n < 0, \\ 2\pi, & \text{for } n = 0, \\ 4\pi, & \text{for } n > 0, \end{cases} \quad (5)$$

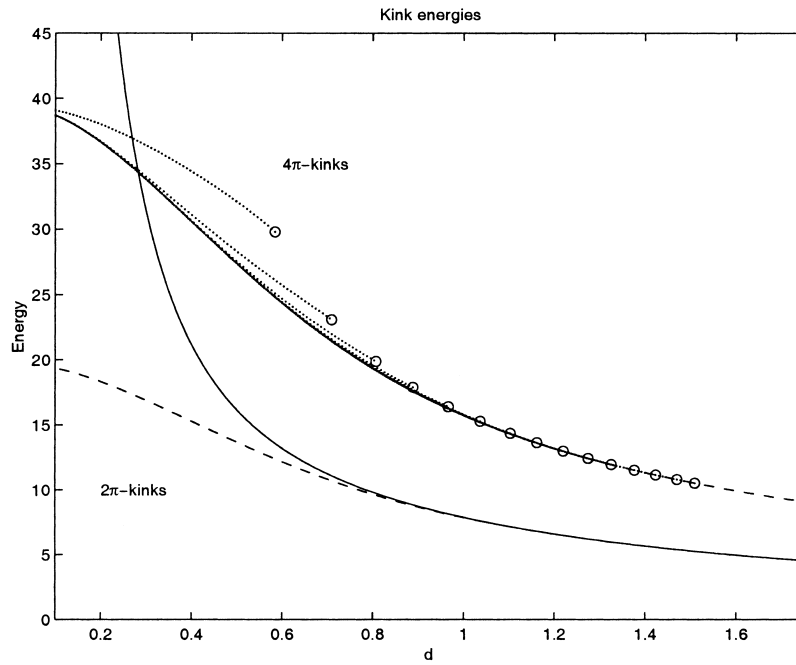


Fig. 1. Energies for 2π -kinks and some 4π -kinks. The centred 2π -kink is shown as the solid line, the off-centred version by the dashed line. The energies of 4π -kinks are shown as dots. These particular kinks are generated by tracing uncoupled equilibria with the structure (7) to larger d . The dashed line that these equilibria largely follow is twice the energy of the off-centred 2π -kink. The circles indicate where these branches of kink solutions end in saddle-node bifurcations. The termination points move to larger d as $N_1 + N_2$ increases.

we generate two types of kinks, off-centred or centred at 2π . Since both are stable at $d = 0$, we expect them to remain stable at small enough d also. But we can also produce a kink from

$$Y_n = \begin{cases} 0, & \text{for } n < 0, \\ \pi \text{ or } 3\pi, & \text{for } n = 0, \\ 4\pi, & \text{for } n > 0, \end{cases} \quad (6)$$

which is unstable, and a whole slew of other, more complicated solutions in which we take the central region of the kink to be more structured.

Evidently, there is a huge number of possible uncoupled solutions that can be continued to finite d . Some particular solution branches are shown in Figs. 1 and 2. The branches resulting from continuing (5) and (6) appear in Fig. 2, along with the kinks given at $d = 0$ by $(\dots, 0, 0, \pi, 2\pi, 3\pi, 4\pi, 4\pi, \dots)$ and $(\dots, 0, 0, \pi, 2\pi, 2\pi, 3\pi, 4\pi, 4\pi, \dots)$, and all those with $(\dots, 0, 0, x_0, x_1, 4\pi, 4\pi, \dots)$, where x_0 and x_1 are all permutations of $0, \pi, 2\pi, 3\pi$ and 4π .

Many of the branches end in saddle-node bifurcations. Fig. 2(a) gives the misleading impression that there appear to be three branches terminating at some of these bifurcations; further inspection shows that there are actually four branches that end at nearby coupling strengths. Two branches terminate in a pitchfork on a third branch just below the saddle node (see panel (b)). This first bifurcation is a symmetry-breaking bifurcation in which two kinks appear without the symmetry $y_n \rightarrow 2\pi - y_{-n}$.

Some other interesting solutions consist, at $d = 0$, of

$$Y_n = \begin{cases} 0, & \text{for } n \leq -N_1, \\ 2\pi, & \text{for } -N_1 < n \leq N_2, \\ 4\pi, & \text{for } n > N_2, \end{cases} \quad (7)$$

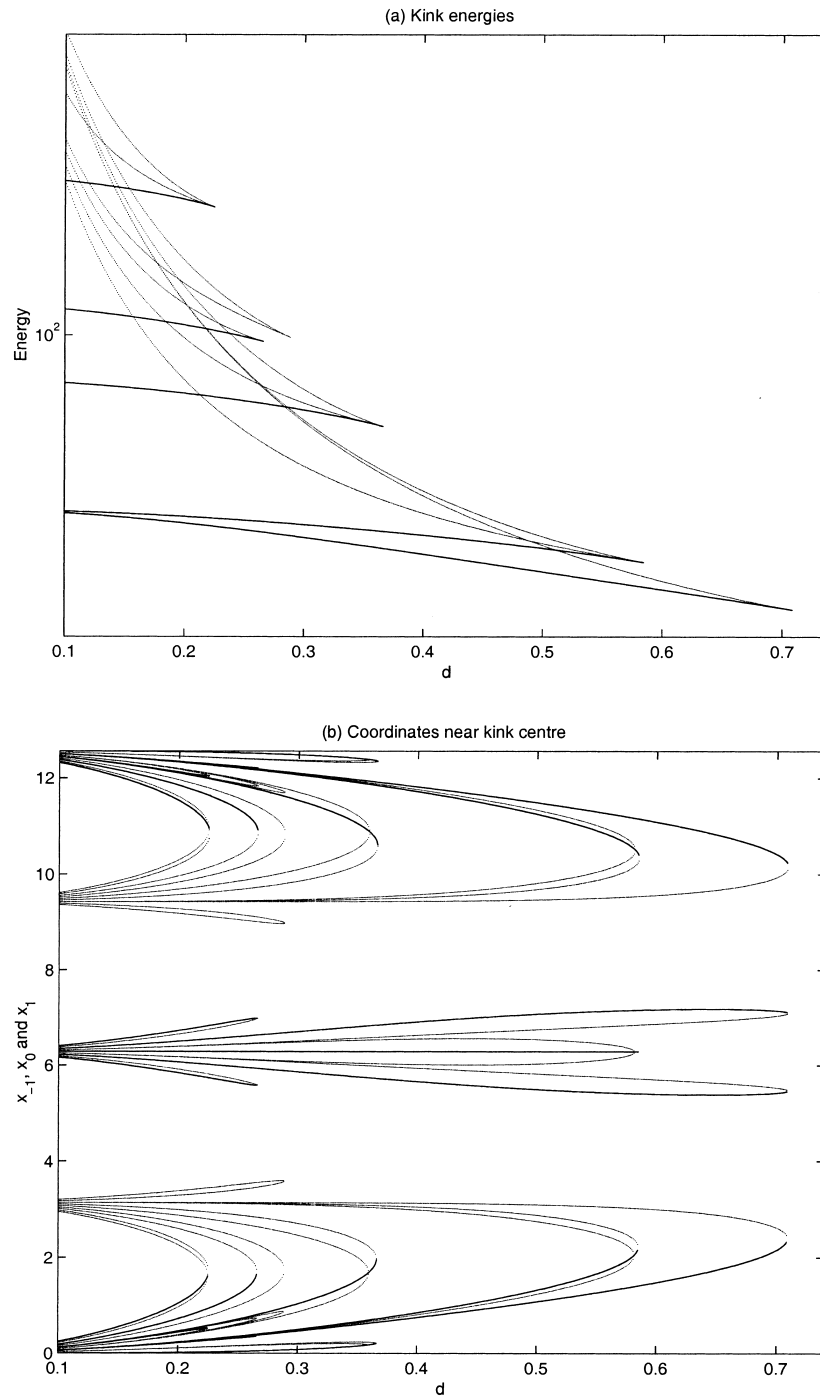


Fig. 2. Panel (a) shows energies of different 4π -kinks as a function of d . Panel (b) shows the coordinates of three oscillator kinks nearest the kink centre. The kinks displayed are constructed by tracing the equilibria given at $d = 0$ by $(\dots, 0, 0, x_0, x_1, 4\pi, 4\pi, \dots)$, where x_0 and x_1 are all permutations of $0, \pi, 2\pi, 3\pi$ and 4π . In addition, the kinks with $(\dots, 0, 0, \pi, 2\pi, 3\pi, 4\pi, 4\pi, \dots)$ and $(\dots, 0, 0, \pi, 2\pi, 2\pi, 3\pi, 4\pi, 4\pi, \dots)$ at $d = 0$ are included. The branches that are stable when they begin at $d = 0$ are drawn as thicker lines.

which take the form of kinks with increasingly wide central “plateaux”. These are again stable at $d = 0$. The first 15 kinks of this form (with $N_2 + N_1 < 16$) are continued to finite d as shown in Fig. 1. These branches again disappear in saddle-nodes. But as the number of oscillators contained in the central plateau increases, the kinks continue to exist at higher d . This is just a consequence of the fact that as we increase the number of lattice sites in the plateau, the two pieces of the kink become widely separated, and the solution develops into individual (off-centred) 2π kinks which exist as stable solutions for arbitrarily large d . But, evidently, the 4π -kink equilibria that persist to the highest coupling strength consist of widely separated 2π -kinks.

3. Stability

The goal of what we are doing is to find the equilibria, and look at their stability. Having found the equilibria by the techniques described above, we now turn to stability. Essentially, we adapt the Evans function analysis to look at the stability of the numerically generated kinks. In general, this technique uncovers instabilities that are localized to the fronts. Here, for example, in the case of $2M\pi$ -kinks with $M > 1$, instabilities can arise that break them apart.

The stability problem is formulated as follows. We perturb the lattice about the stationary kink:

$$y_n(t) = Y_n + u_n(t), \tag{8}$$

where Y_n denotes the equilibrium kink. After introducing this decomposition into the governing equation and linearizing in u_n , we find

$$\ddot{u}_n = u_{n+1} + u_{n-1} - 2u_n - \frac{u_n}{d^2} \cos Y_n. \tag{9}$$

The eigenvalue spectrum is determined by taking $u_n \propto \exp \lambda t$ and applying the boundary conditions, $u_n \rightarrow 0$ as $n \rightarrow \pm\infty$.

We then have:

$$\lambda^2 u_n = u_{n+1} + u_{n-1} - 2u_n - \frac{u_n}{d^2} \cos Y_n. \tag{10}$$

This is an infinite dimensional matrix problem. However, it is real and symmetric. Thus eigenvalues must arise as either real pairs or imaginary pairs; there are no quartets as can occur in other Hamiltonian systems. This severely constrains the types of instabilities that can occur, and indicates that the passage to instability always takes place through the origin.

3.1. Evans functions

To the left of the kink, the amplitude of Y_n decays exponentially quickly to zero. Similarly, $Y_n \rightarrow 2M\pi$ to the right. Hence

$$n \rightarrow \pm\infty : \left(\lambda^2 + \frac{1}{d^2} \right) u_n \sim u_{n+1} + u_{n-1} - 2u_n. \tag{11}$$

This linear system has solutions

$$u_n = C_{\pm}(\lambda)r_1^n + D_{\pm}(\lambda)r_2^n \equiv C_{\pm}(\lambda)e^{v_1 n} + D_{\pm}(\lambda)e^{v_2 n}, \tag{12}$$

where $C_{\pm}(\lambda)$ and $D_{\pm}(\lambda)$ are independent of n and

$$r_{2,1} = \frac{1}{2} \left[\lambda^2 + 2 + \frac{1}{d^2} \pm \sqrt{\left(\lambda^2 + \frac{1}{d^2} \right) \left(\lambda^2 + 4 + \frac{1}{d^2} \right)} \right] \quad \text{or} \quad v_{2,1} = \pm \sin^{-1} \sqrt{\lambda^2 + \frac{1}{d^2}} \quad (13)$$

(so that $v_1 < 0$ and $v_2 > 0$).

We may begin the construction of an eigenfunction to the left by setting $C_-(\lambda) = 0$; then

$$u_n \sim D_-(\lambda) r_2^n = D_-(\lambda) e^{v_2 n} \quad \text{for } n \rightarrow -\infty. \quad (14)$$

On taking a specific choice for $D_-(\lambda)$, we begin an iteration of (10) from large, negative values of n , progress through the kink (centred at or near $n = 0$), then out to large, positive values of n . At that stage, for general λ , the solution takes the form,

$$u_n \sim C_+(\lambda) r_1^n + D_+(\lambda) r_2^n = C_+(\lambda) e^{v_1 n} + D_+(\lambda) e^{v_2 n}. \quad (15)$$

Crucially, u_n , diverges unless $D_+(\lambda) = 0$. This coefficient is equivalent to the transmission coefficient of a wave-scattering problem, and depends upon λ . The function $D_+(\lambda)$ is only zero if λ is an eigenvalue, thus the function $D_+(\lambda)$ and its determination encapsulates the eigenvalue problem. Explicitly, if we continue the iteration to $n = L$ then

$$D_+(\lambda) = \frac{u_{L+1} - r_1 u_L}{r_2^{L+1} - r_2^L r_1} \equiv \frac{r_2 u_L - u_{L-1}}{r_2^{L-1} (r_2^2 - 1)}, \quad (16)$$

where we use the relations,

$$r_1 r_2 = 1, \quad u_{L+1} = \chi u_L - u_{L-1}, \quad \chi = 2 + \frac{1}{d^2} + \lambda^2 \quad (17)$$

(which hold to within an exponentially small error if $n = L$ is sufficiently far from the centre of the kink).

The coefficient $D_+(\lambda)$ is essentially our dispersion relation. Should $D_+(\lambda) = 0$, then the solution decays exponentially to both right and left, and we have an eigenmode. As it stands this coefficient clearly has the analytic structure of $r_{1,2}$, together with any structure that we add into the coefficient $D_-(\lambda)$. Notably, $r_{1,2}$ have branch points at $\lambda = \pm i/d$ and $\pm i\sqrt{4 + 1/d^2}$; to connect these points we take the branch cuts, $[i/d, i\sqrt{4 + 1/d^2}]$ and $[-i/d, -i\sqrt{4 + 1/d^2}]$.

These branch cuts locate the continuous spectrum of the kink; it is not difficult to show that along these spectral cuts, there is no spatially decaying linear solution. The cuts of the continuum correspond to the ‘‘phonon frequency band’’.

For technical reasons it is convenient to select the initial function $D_-(\lambda)$ such that $D_+(\lambda)$ has a special form for large $|\lambda|$, namely unity. In order to find a suitable choice we note that for large $|\lambda|$, an approximate solution to (10) follows using $r_1 \sim \lambda^2$, $r_2 \sim \lambda^2$ and

$$u_{n+1} = \lambda^2 u_n. \quad (18)$$

This indicates that, if we begin on the left at $n = -L$, then continue through the kink up to $n = +L$,

$$D_+(\lambda) \sim \lambda^{4L} D_-(\lambda). \quad (19)$$

By taking $D_-(\lambda) = r_1^{2L} \sim \lambda^{-4L}$, the transmission coefficient, $D_+(\lambda)$, therefore approaches unity on the right.

A second technicality concerns the denominator in (16). This denominator introduces poles into $D_+(\lambda)$ at the zeros of r_2^{L-1} and $1 - r_2^2$. However, because $r_1 r_2 = 1$, there are no zeros of the first quantity in the finite complex

plane. But the second factor of the denominator vanishes for $r_2 = \pm 1$, which occurs at the branch points of the continuous spectrum. Though this does not directly affect the analytic structure of $D_+(\lambda)$, it does obscure the Nyquist theory that we describe below, and it is convenient to explicitly remove these poles from the transmission coefficient. We do this by scaling $D_-(\lambda)$ with the factor $(r_2^2 - 1) / r_2^2 \equiv (1 - r_1^2)$, which leaves the large λ form of $D_+(\lambda)$ unchanged. Overall, the analytic structure of $D_+(\lambda)$ remains that of $r_{1,2}$. Thus, with this selection of $D_-(\lambda)$, we let $D_+(\lambda) = \mathcal{D}(\lambda)$, the *Evans function*.

3.2. Nyquist theory

Now, $\mathcal{D}(\lambda)$ is a complex function that is analytic over the complex plane, but for branch cuts that locate the continuous spectrum. Moreover, $\mathcal{D}(\lambda) \rightarrow 1$ as $|\lambda| \rightarrow \infty$. Thus, if we define a region of the complex plane with perimeter \mathcal{C} that does not contain either of the branch cuts, Cauchy’s residue theorem tells us that the integral defined by

$$N_c = \frac{1}{2\pi i} \int_{\mathcal{C}} \frac{\mathcal{D}'(\lambda)}{\mathcal{D}(\lambda)} d\lambda \tag{20}$$

is equal to the number of zeros of $\mathcal{D}(\lambda)$ inside the contour \mathcal{C} . In particular, if \mathcal{C} is a semicircle of infinite radius enclosing the right-half plane,

$$N_c = \frac{1}{2\pi i} \int_{\epsilon - i\infty}^{\epsilon + i\infty} \frac{\mathcal{D}'(\lambda)}{\mathcal{D}(\lambda)} d\lambda \tag{21}$$

counts the number of zeros with $Re(\lambda) > \epsilon$, as $\epsilon \rightarrow 0$. This determines the number of unstable eigenmodes.

By the argument principle, the integral is equal to the integral change of phase of $\mathcal{D}(\lambda)$ as λ varies along \mathcal{C} . Equivalently this is the number of times the curve $\mathcal{D}(\lambda)$ winds around the origin on the $(\mathcal{D}_r, \mathcal{D}_i)$ -plane. Thus we can visualize the behaviour of $\mathcal{D}(\lambda)$ conveniently and the procedure becomes standard Nyquist technology; an example is shown in Fig. 3.

This figure shows that the centred kink is unstable, but the off-centred one is stable (a known result, and one anticipated by the stability at $d = 0$). This is seen from the final magnification which shows how the tortuous path of the Nyquist plot eventually skirts to the right of the origin in the off-centred case, leading to no enclosures. However, the centred kink circles around the origin, implying instability.

In other words, the centred kink possesses two purely real eigenvalues, a growing–decaying mode pair. The spectrum of the off-centred kink, on the other hand, lies along the imaginary axis. In fact, for the off-centred kink, there are two discrete modes lying on the imaginary axis in addition to the continuous spectrum. This pair, and the real pair of the centred kink, can be thought of as resulting from the breaking of the translational symmetry of the sine-Gordon equation by discretization. The imaginary eigenvalues of the off-centred kink are “pseudo-Goldstone” modes (the translational symmetry of the continuous system leads to a purely neutral, translation mode in the linear eigenspectrum; this mode is often referred to as the Goldstone mode). For the off-centred kink, the frequency of the pseudo-Goldstone modes is shown in Fig. 4; the eigenvalue decays roughly exponentially with d . Also, as indicated in Fig. 4, there is a further pair of imaginary eigenvalues for the off-centred kink that exist over a limited range in d ; we return to these “shape modes” in Section 3.4.

3.3. Remarks on the Evans functionology and Nyquist technology

There are several useful general features of the Evans functions and Nyquist plots that expedite the determination of stability. First, because λ^2 appears in the iteration equation (10), the Nyquist plots are symmetrical under reflection about the real axis.

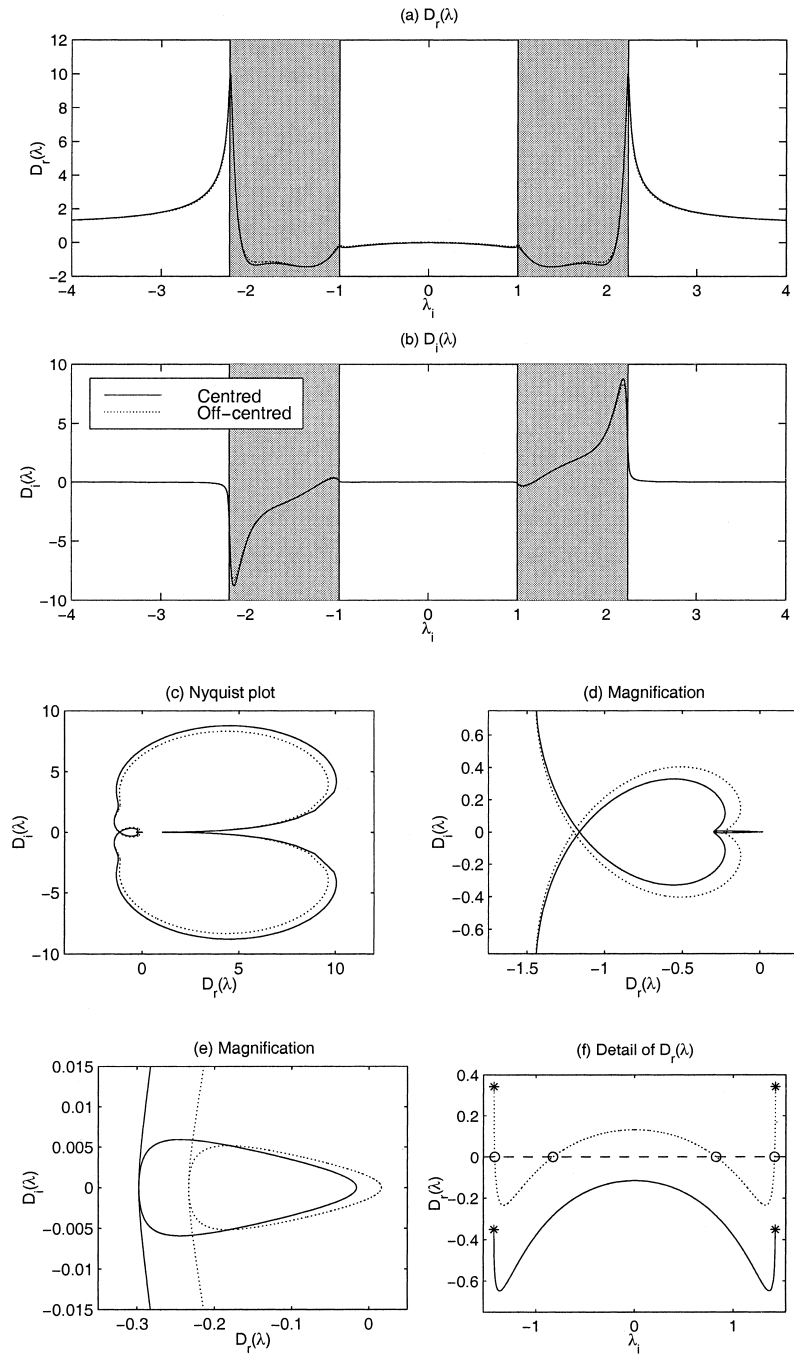


Fig. 3. Panels (a) and (b) show Evans functions for 2π -kinks with $d = 1$, and (c)–(e) show Nyquist plots. A rather large value of ϵ is used ($\epsilon = 10^{-2}$) to reveal the structure more easily. The shaded regions in (a) and (b) denote the continuum bands. In panel (f) we display $\mathcal{D}_r(\lambda)$ for λ over the imaginary axis between $-1/d$ and $1/d$, with $d = 0.7$ and $\epsilon = 10^{-10}$. Stars indicate the value of $\mathcal{D}_r(\lambda)$ beside the branch points of the continuous spectrum, and circles indicate zero-crossings.

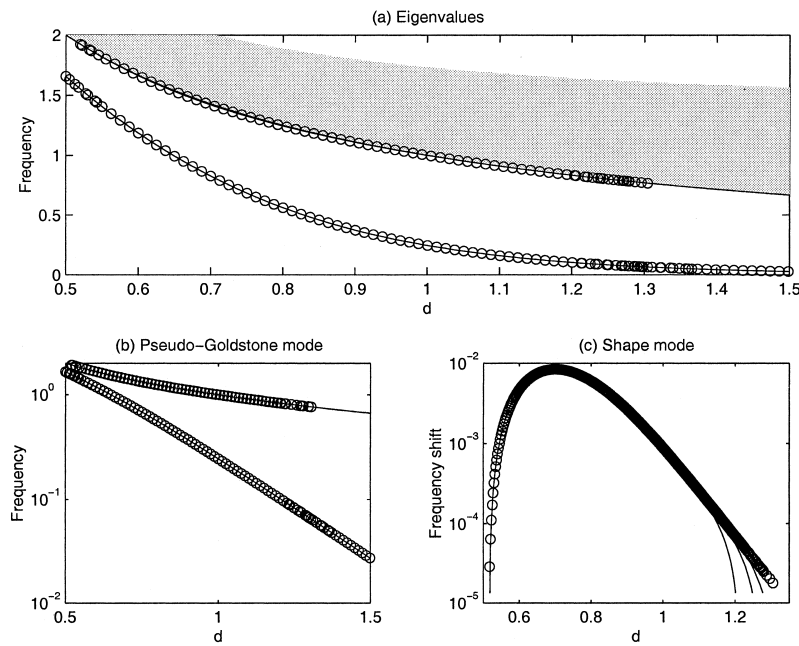


Fig. 4. Discrete modes of the off-centred, 2π -kink. Panels (a) and (b) show circles locating the frequencies, ω , of the discrete modes computed by finding the zeros of the Evans function by Newton iteration. The lines that track the circles are the two lowest eigenfrequencies as computed from the stability matrix resulting from assuming that perturbation displacements vanish at the ends of the computational lattice; the two sets of eigenvalues are practically indistinguishable. The shaded region shows the frequency range occupied by the continuous spectrum. Panel (c) shows the frequency shift of the “shape mode” discussed in Section 3.4 from below the lower edge of the continuum ($1/d - \omega$). In (c), the three solid lines reflect results for the second approximate method with different lattice sizes (200, 300 and 400).

Second, and perhaps most importantly, because instability always proceeds through the origin, it is sufficient to monitor $\mathcal{D}(0) < 0$ in order to detect instability. Indeed, $\mathcal{D}(0) < 0$ is a sufficient condition for instability for the example used above, where there is the possibility of one unstable mode. However, when there may be multiple instabilities, $\mathcal{D}(0)$ must necessarily cross through zero repeatedly. This obscures that simple picture, and more knowledge of the Nyquist curve is needed. In Fig. 5 we display the Evans function $\mathcal{D}(0)$ for the two 2π -kinks also shown in Fig. 3; one (the centred kink) has $\mathcal{D}(0) < 0$ implying instability.

More examples are shown in Figs. 6 and 7. The first picture displays eigenvalues and Evans functions for one of the 4π -kinks shown in Fig. 2. The bifurcation diagram suggests that the branch that is tracked from the uncoupled limit is initially stable, but then bifurcates to instability in a symmetry-breaking bifurcation just before it disappears in a saddle node. This sequence is confirmed by tracking the eigenvalues (panel (a)) and by plotting the Evans function $\mathcal{D}(0)$ (panel (b)).

Third, one negative aspect of the Nyquist plots is that they can be very convoluted; the curve often loops many times, with many tight turns near the origin that require several successive magnifications (see Fig. 3). This makes it difficult to pick out the number of enclosures. However, we may automate the identification of encirclings by noting that the integral in (21) is equivalent to $\ln \mathcal{D}$ evaluated at the beginning and end of the contour \mathcal{C} . As a function of $\mathcal{D} = \mathcal{D}_r + i\mathcal{D}_i$, this quantity has a branch cut along $\mathcal{D}_i = 0$ and $\mathcal{D}_r < 0$. The change of phase of $\mathcal{D}(\lambda)$ arises as the Nyquist curve passes through that branch cut and begins and ends on different Riemann sheets of the \ln function. Thus to determine the change of phase we record the crossings of the real axis to the right of the origin, noting the sense of crossing, and hence the passage onto either an upper or lower Riemann sheet:

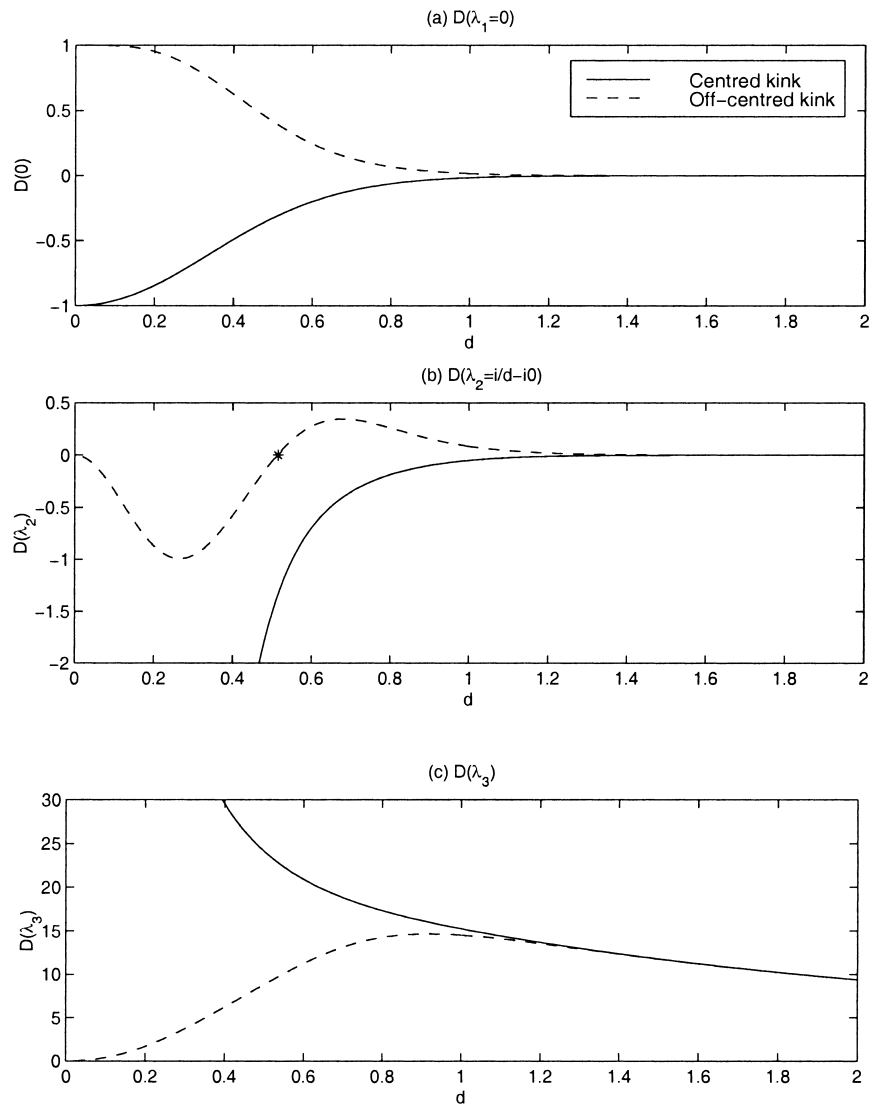


Fig. 5. Evans functions for 2π -kinks: (a) $\mathcal{D}(0)$, (b) $\mathcal{D}(\lambda_2 = i/d - i0)$ and (c) $\mathcal{D}(\lambda_3)$, where $\lambda_3 = i(4 + l/d^2)^{1/2} + i0$ lies just above the upper limit of the continuous spectrum.

$$\frac{1}{2\pi i} \Delta \arg \mathcal{D} = \sum \operatorname{sgn} \left(\frac{\partial \mathcal{D}_i}{\partial \lambda} \right)_{\mathcal{D}_i=0, \mathcal{D}_r < 0}. \quad (22)$$

This yields the number of encirclings.

Lastly, along the real axis, away from the branch cuts of the continuous spectrum, r_1 and r_2 are real. Consequently, $\mathcal{D}_i(\lambda) = 0$ along these sections of the locus of λ . Moreover, here, the Evans function is analytic, so we may Taylor expand to find:

$$\mathcal{D}_i(ix) = \epsilon \frac{d\mathcal{D}_r(ix)}{dx}, \quad (23)$$

for $\lambda = ix + \epsilon$.

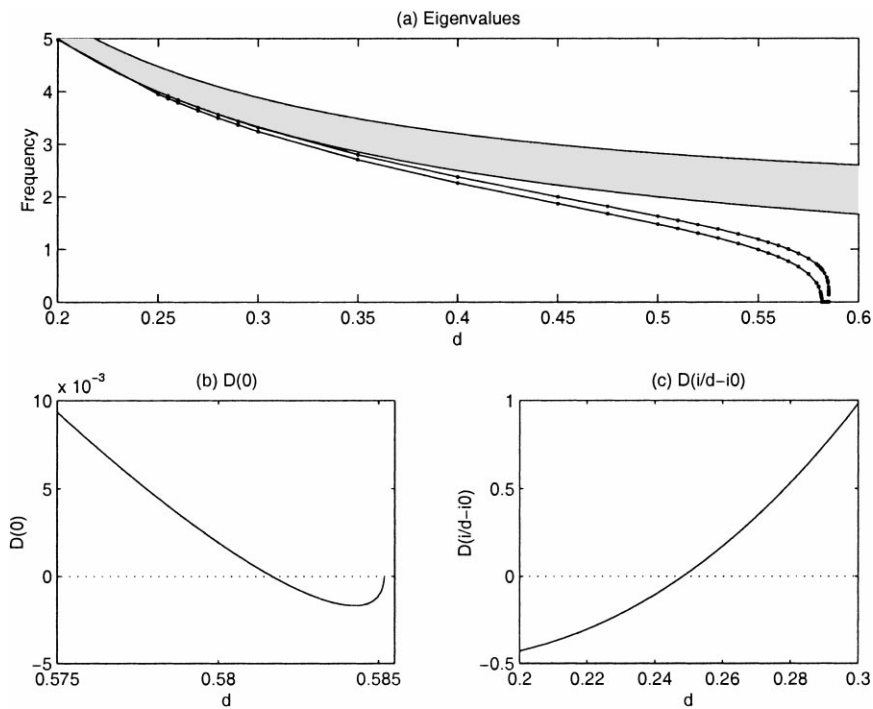


Fig. 6. Eigenvalues and Evans functions for a 4π -kink. At $d = 0$, this kink has the structure, $(\dots, 0, 2\pi, 4\pi, \dots)$. Panel (a) shows the frequency of two discrete modes (one of which disappears near $d = 0.25$) and the continuum band as a function of d . Panels (b) and (c) show the Evans functions, $\mathcal{D}(0)$ and $\mathcal{D}(i/d - i0)$.

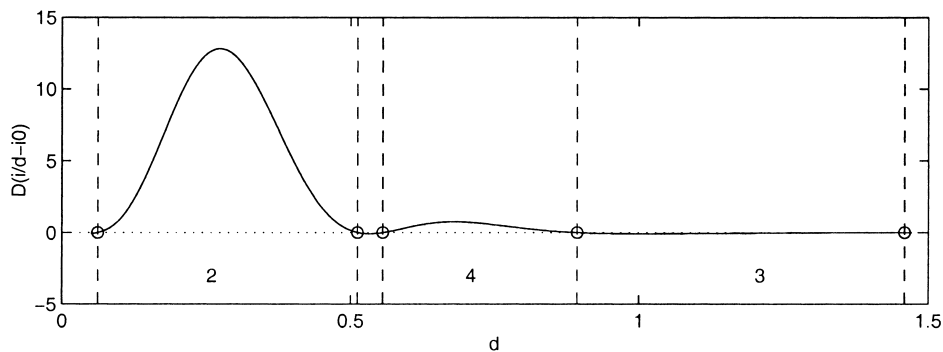


Fig. 7. Evans function $\mathcal{D}(i/d - i0)$ for a 4π -kink given, at $d = 0$, by (7) with $N_1 + N_2 = 11$. Circles indicate zero-crossings and the numbers refer to the number of shapes modes supported by the structure over that range of d .

On a more technical note, it is evident from Fig. 4 that Evans functions and Nyquist methods are not the only simple means of detecting stability. In this picture we compare the eigenvalues determined as zeros of the Evans functions with frequencies determined by a more direct, approximate method. In this method, we assume that the lattice has a finite size and adopt the boundary conditions that the perturbation displacements vanish at the ends; the eigenvalues then follow as those of a matrix of finite size. This computational procedure (used also by Braun et al. [18]) is less accurate in its treatment of the tails of the kink and its linear eigenmodes. As a result, it fails to

treat the continuous spectrum properly and instead represents this portion of the spectrum as a dense collection of discrete modes whose separation decreases with the size of the matrix. But nevertheless, provided the computational domain is sufficiently large, the discrete eigenvalues so determined agree with the zeros of the Evans function (the two are indistinguishable in the picture). However, as we indicate next, Evans functions reveal features of the linear eigenspectrum that one cannot extract with these other techniques.

3.4. Internal shape modes

Several studies of the sine-Gordon equation and its relatives have outlined the importance of intrinsic modes of vibration of the kink [18,19]. These modes appear in the linear eigenspectrum as additional discrete eigenvalues (Fig. 4). Their presence is also detectable using Evans functions.

One such pair of modes is evident in the final panel of Fig. 3. This figure displays $\mathcal{D}_r(\lambda)$ over the central portion of the path of λ . In this case, with $\epsilon \rightarrow 0$, the zero-crossings of $\mathcal{D}_r(\lambda)$ reflect modes that lie on the imaginary axis. For the off-centred kink, there are two pairs of crossings. The first pair, at $\lambda \approx \pm i0.827$ are the pseudo-Goldstone modes. The others, $\lambda \approx i1.420$, lie just outside the continuous spectrum (see Fig. 4).

One curious aspect of the shape modes is that they do not exist for all d . In fact, as we lower the coupling strength, the shape modes revealed in Fig. 3(f) disappear by entering the continuous spectrum through the branch point at $\lambda = \pm i/d$. This is a novel type of bifurcation from the continuous spectrum, one previously studied in [25]. Because the shape modes appear (or disappear) by detaching from the continuous spectrum, they are detected by looking at the value of the Evans function as λ limits to the branch points from outside the continuum; that is, from $\mathcal{D}(i/d - i0)$ and $\mathcal{D}(i\sqrt{4 + 1/d^2} + i0)$. These functions are shown in Fig. 5. At the zero crossings of this function, the shape modes appear through the branch points.

The rescaling of $D_-(\lambda)$ adopted earlier to generate the Evans function $\mathcal{D}(\lambda)$ has some significance for this computation: we rescale using a quantity that vanishes at the branch points in order to explicitly remove the poles that would otherwise occur there. However, the main idea is that $\mathcal{D}(\lambda)$ also contains a zero at a point that gradually moves along the imaginary axis as we vary parameters. At the point of bifurcation the zero coincides with the pole at the branch point, and this leads to a finite value of the Evans function after an appropriate continuation argument. Equivalently, we detect the occurrence of that finite value by monitoring $\mathcal{D}(i/d - i0)$ or $\mathcal{D}(i\sqrt{4 + 1/d^2} + i0)$.

For the off-centred 2π -kink, the function $\mathcal{D}(\lambda_2 = i/d - i0)$ passes through zero near $d \approx 0.515$ (see Fig. 5). For d greater than this value, the shape modes appear out of the lower branch points as discrete modes. A similar bifurcation occurs for the 4π -kink represented in Fig. 6, as revealed in panel (c). Note that we never observed any shape modes to detach from the upper edges of the continuum (cf. Braun et al. [18]); the Evans function $\mathcal{D}(i\sqrt{4 + 1/d^2} + i0)$ invariably appeared to have one sign.

Importantly, the Evans function clearly reveals that the shape modes continue to exist at larger d for the off-centred 2π -kink. However, it becomes impossible from a numerical perspective to find these modes explicitly when d is much above 1.3. This is shown in panel (c) of Fig. 4, which displays the frequency shift of the shape mode from below the lower branch point of the continuum; for larger d it becomes too close to the continuum to find without an excessive increase in the size of the lattice used in the computation (presumably for this reason, Braun et al. reported the mode as existing only up to $d \approx 1.2$).

An even more interesting bifurcation structure is shown in Fig. 7, which shows the Evans function $\mathcal{D}(i/d - i0)$ for a kink of the form (7) at $d = 0$ and $N_1 + N_2 = 11$. This kink is stable over almost the whole range over which the solution exists. But near the saddle node at which the kink disappears, there is a loss of stability much like that revealed in Fig. 6. However, there are several bifurcations of shape modes over this range in coupling strength. First, as we raise d , three complex conjugates appear in Fig. 7, leading to a total of four pairs. Then two of these successively disappear, leaving two pairs of shape modes that each resemble the pair of the 2π -kink (which

is expected at this stage, since the kink closely resembles two well-separated 2π -kinks). The two pairs of shape modes that exist for $0.55 < d < 0.9$ may well be rationalized in terms of kink interactions.

3.5. Kink depinning

There are apparently two generic features of the 4π -kinks that have increasingly wide plateaux at their centres. First, as shown in Fig. 1, the corresponding solution branches terminate in saddle nodes at successively higher coupling strengths. Second, shortly before that termination, the kinks all appear to lose stability. We briefly digress from the issue of linear stability in order to determine the fate of the kinks that lose stability in this way. In order to do this, we conduct some numerical simulations of the sine-Gordon lattice, starting from initial conditions close to the unstable kinks. Two sample results are shown in Fig. 8. In the first example, the two pieces of the kink drift apart and settle into a vacillation around a neighbouring equilibrium kink with a slightly wider plateaux (one that is still stable at that value of d). That vacillation is partly described by the shape modes considered above. A significant amount of radiation is also generated and propagates to the edges of the domain.

In the second example there is little radiation generated and the two parts of the kink drift apart, leading to a stationary 2π -kink and a moving one. The latter presumably generates low amplitude radiation that will eventually damp its motion and pin it. In other words, the loss of stability of the 4π -kink at this stage leads to two widely separated 2π -kinks.

These experiments suggest that as we begin from $d = 0$, these 4π -kinks gradually split into two 2π -kink components. At larger d , the radiation that brakes moving kinks becomes so slight that the components can drift well apart.

3.6. Analytical results for approximate, highly discrete kinks

Finally, we mention some analytical results for stability. These are based on an approximation to the lattice equations that is valid when d is small.

In the limit $d \rightarrow 0$, the system becomes highly discrete and the kink consists of a jump from the left asymptotic value to the right asymptote across just a few lattice points. In this instance, we may build kink solutions by asymptotic means; these are kinks for which the elements all lie at the values 0 or $2M\pi$, but for a small number of elements lying near the kink centre. The computation of the kink profile then reduces to finding the amplitudes in these distinguished elements.

Rather than follow the asymptotic route, we take a short-cut (reminiscent of a Galerkin truncation) and consider a kink with a given number of distinguished elements, simply ignoring the errors that occur elsewhere along the lattice. We select the *four-point* kink by way of example. This kink has the distinguished sites, $n = -2, -1, 0$ and 1 . Then, $Y_n = 0$ for $n < -2$ and $Y_n = 2M\pi$ for $n > 1$. The mean lattice values satisfy

$$d^2(2\pi + Y_0 - 2Y_1) = \sin Y_1, \quad d^2(Y_1 + Y_{-1} - 2Y_0) = \sin Y_0 \tag{24}$$

and

$$d^2(Y_0 + Y_{-2} - 2Y_{-1}) = \sin Y_{-1}, \quad d^2(Y_{-1} - 2Y_{-2}) = \sin Y_{-2}, \tag{25}$$

which constitutes an algebraic problem for the Y_j 's.

By following the route laid out above, we construct the Evans function. After some algebra we obtain:

$$\mathcal{D}_4 = (1 - r_1 \Lambda_{-2})(1 - r_1 \Lambda_{-1})(1 - r_1 \Lambda_0)(1 - r_1 \Lambda_1) - r_1^2 [1 + r_1^2 \Lambda_1 \Lambda_{-2} (r_1 \Lambda_0 + r_1 \Lambda_{-1} - 1 - r_1^2) - r_1^2 (\Lambda_0 \Lambda_{-2} + \Lambda_1 \Lambda_{-1})], \tag{26}$$

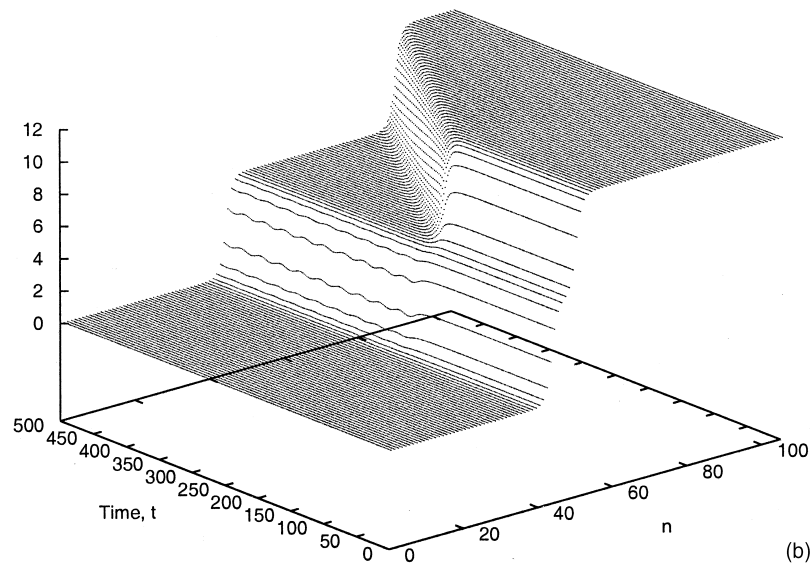
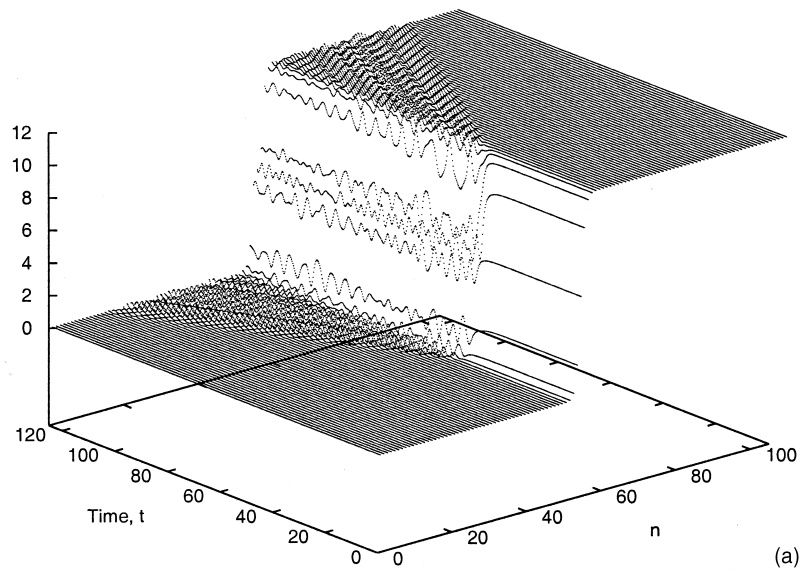


Fig. 8. Initial-value problems at (a) $d = 0.584$ and (b) $d = 1.0375$. Shown are values of $y_n(t)$ against n and t at intervals of 0.25 and 2, respectively.

where

$$\Lambda_j = \frac{1}{d^2}(1 - \cos Y_j). \quad (27)$$

One class of four-point kinks is symmetrical with $Y_{-2} = 2M\pi - Y_1$ and $Y_{-1} = 2M\pi - Y_0$. This indicates that $\Lambda_1 = \Lambda_{-2}$ and $\lambda_0 = \Lambda_{-1}$ and the formula for \mathcal{D}_4 simplifies somewhat.

We may extract simpler expressions from this formula for kinks with fewer distinguished sites simply by setting various of the Λ_j 's to zero. For example, for the three-point kink occupying the sites $n = -1, 0$ and 1 ,

$$\mathcal{D}_3 = (1 - r_1 \Lambda_{-1})(1 - r_1 \Lambda_0)(1 - r_1 \Lambda_1) - r_1^2(1 - r_1^2 \Lambda_1 \Lambda_{-1}). \tag{28}$$

For symmetrical three-point kinks $Y_{-1} = 2M\pi - Y_1$ and $Y_0 = M\pi$. Hence $\Lambda_1 = \Lambda_{-1}$, and so

$$\mathcal{D}_3 = (1 - r_1 \Lambda_1)[(1 - r_1 \Lambda_0)(1 - r_1 \Lambda_1) - r_1^2(1 + r_1 \Lambda_1)]. \tag{29}$$

After even more simplification, we reduce to the two-point kink over $n = -1$ and 0 :

$$\mathcal{D}_2 = (1 - r_1 \Lambda_{-1})(1 - r_1 \Lambda_0) - r_1^2. \tag{30}$$

This time symmetry demands $Y_{-1} = M\pi - Y_0$, so $\Lambda_0 = \Lambda_{-1}$ and

$$\mathcal{D}_2 = (1 - r_1 \Lambda_0)^2 - r_1^2. \tag{31}$$

In this second case we may explicitly find the eigenvalues by solving a quadratic (cf. Braun et al. [18]).

To compare the analytic versions of the Evans functions with those constructed numerically above, we explicitly consider the symmetrical, 3-point, 4π -kink. This kink is given by $Y_{-1} = Y_1 = a$ and $Y_0 = 2\pi$, where

$$2d^2(\pi - a) = \sin a. \tag{32}$$

There are various solutions to this transcendental equation, each giving various kink structures. In particular, there is a kink with $a = 0$ at $d = 0$, that corresponds to the 4π -kink shown in Figs. 1, 2 and 6. The solution to (32) increases with d up to $d = 1/\sqrt{2} \approx 0.707$, where it disappears. This value should be compared with $d \approx 0.58$, the saddle-node bifurcation point of the numerically constructed kink. Though the two values compare relatively well, the 3-point kink actually ends in a pitchfork bifurcation rather than a saddle node, and so the bifurcation structure is qualitatively wrong.

This 3-point kink has the Evans function,

$$\mathcal{D} = (1 - r_1 \Lambda)[(1 - r_1^2) - r_1 \Lambda(1 + r_1^2)], \tag{33}$$

where $\Lambda = (1 - \cos a)/d^2$. From this formula, we may extract the Evans functions, $\mathcal{D}(0)$, $\mathcal{D}(i/d)$ and $\mathcal{D}(i\sqrt{4 + 1/d^2})$. The results are shown in Fig. 9. Again, somewhat surprisingly, the results agree with the numerical computations in Fig. 6, showing the bifurcation of a shape mode near $d = 0.25$ and a loss of stability shortly before the termination of the branch.

In fact, the shape mode eigenvalue factorizes cleanly out of the Evans function in (33):

$$\mathcal{D} = \mathcal{D}_s \mathcal{D}_g, \quad \text{where } \mathcal{D}_s = 1 - r_1 \Lambda \quad \text{and} \quad \mathcal{D}_g = (1 - r_1^2) - r_1 \Lambda(1 + r_1^2). \tag{34}$$

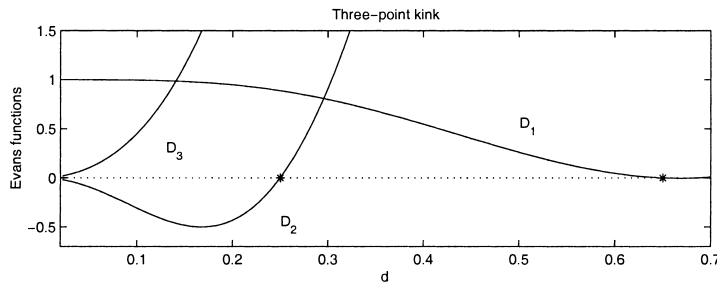


Fig. 9. Evans functions, $\mathcal{D}_1 = \mathcal{D}(0)$, $\mathcal{D}_2 = \mathcal{D}(i/d - i0)$ and $\mathcal{D}_3 = \mathcal{D}(i[4 + 1/d^2]^{1/2} + i0)$ for the symmetrical, three-point, 4π -kink. The stars indicate zero-crossings.

The first factor, \mathcal{D}_s , is that part of the Evans function corresponding to the shape mode. Provided $\Lambda < 1$ we may explicitly solve $\mathcal{D}_s = 0$:

$$1 = r_1 \Lambda \quad \text{or} \quad \omega^2 = 2 + \frac{1}{d^2} - (\Lambda + \Lambda^{-1}). \quad (35)$$

This frequency coincides with the lower edge of the continuum when $d \approx 0.2497$ and $a \approx 0.355$ (and does not exist for $\Lambda < 1$ and lower d , since $|r_1| < 1$).

The second factor, \mathcal{D}_g , gives another discrete mode satisfying

$$\omega^2 = 2 + \frac{1}{d^2} - \left(r + \frac{1}{r}\right) \quad \text{and} \quad 1 - r^2 = r\Lambda(1 + r^2). \quad (36)$$

This is the pseudo-Goldstone mode. It is straightforward to show that there is always one solution for r in the range $[0, 1]$. For $d < 0.65$, the eigenvalue is imaginary and the kink is stable. But just above this value, the eigenvalue is real and the kink loses stability, in agreement with the results of Fig. 9.

4. Bisection methods

In the previous section we have outlined the construction of an Evans function for stationary solutions of the discrete sine-Gordon equation. The procedure is much the same for more general systems. However the stability condition embodied in the sign of $\mathcal{D}(0)$ mentioned in Section 3.3 can also be derived in a different way. This alternative method is based on the bisection method for the determination of eigenvalues for symmetric, tridiagonal matrices [20,21]. A similar method has been proposed by Baesens et al. [22] for determining when eigenvalues detach from the continuous spectrum.

For finite dimensional matrices this method surrounds the construction of the leading principal minors p_j of order j , defined by the system of difference equations,

$$p_{n+1}(v) = (A_n - v)p_n(v) + B_n p_{n-1}(v) \equiv \left(2 + \frac{1}{d^2} \cos Y_n - v\right) p_n(v) - p_{n-1}(v), \quad (37)$$

where A_n , and B_n , are the diagonal and off-diagonal entries of the matrix and v is a fixed parameter. This system is in fact identical to our linear stability equations if $v = -\lambda^2$. For computational reasons it is often useful to let $s_n = p_n/p_{n-1}$. This turns the equation into

$$s_{n+1} = \left(2 + \frac{1}{d^2} \cos Y_n - v\right) - 1/s_n \quad (38)$$

and this is the same equation that one would obtain for the pivots in a Gaussian elimination scheme.

For a finite matrix, we begin from the initial condition given by the first entry of the matrix $p_1 = A_1$. Evidently we might use a similar procedure here if we truncated our lattice at finite values of n to both sides of the kink and applied boundary conditions of vanishing perturbation displacement (in the same way the matrix eigenvalue problem was solved in Fig. 4). However we prefer to continue in the same vein set out by the Evans method and make as few approximations as possible in dealing with the infinite kink. Thus we need to generalize the bisection method to infinite matrices.

Because the kink is localized the stability matrix converges to constant entries to the far left and right of the kink, and

$$s_{n+1} \sim 2 + \frac{1}{d^2} - 1/s_n \quad (39)$$

for $|n| \gg 1$. This simple difference equation has two fixed points, namely $s_n = r_1$ and r_2 , in the notation of Section 3. In fact, it is straightforward to see that $s_n = r_2$ is a stable fixed point of the map (39). This means that to the right of the front the s_n s converge to r_2 for a general initial condition, but this does not help us in initiating that initial-value computation.

To initiate the construction of S_n , we argue that as $n \rightarrow -\infty$ the s_n should remain bounded. The only option for such a condition is that $s_n \sim r_2$ as $n \rightarrow -\infty$. Thus in a way akin to our Evans function analysis we can take $p_n = r_2^n$ for some $n = -L$ with L sufficiently large, and use this as the initial value. Alternatively $s_{-L} = r_2$, and we can express the solution to (39) as a continued fraction (in the same fashion we could also write down an explicit continued fraction for the Evans function).

Now, the key argument in the bisection method is that the number of eigenvalues μ of our matrix with $\mu < \nu$ is determined by the number of sign changes of the sequence $(\dots, p_{n-1}, p_n, p_{n+1}, \dots)$. Or, equivalently, the number of negative elements of $(\dots, s_{n-1}, s_n, s_{n+1}, \dots)$. In particular, if $\nu = 0$ the number of sign changes in the sequence p_n is simply the number of unstable modes.

Examples of the construction of the s_n sequence are shown in Fig. 10. This picture reproduces results found with Evans functions.

4.1. Connections with the Evans function

To connect the bisection method described above with our Evans functionology we first notice that the equation for $p_n(\nu = 0)$ is the same as our linear stability equation with $\lambda = 0$, and

$$\mathcal{D}(\lambda = 0) = \left(r_2 - \frac{1}{s_L} \right) \frac{u_L}{r_2^{L-1}}. \tag{40}$$

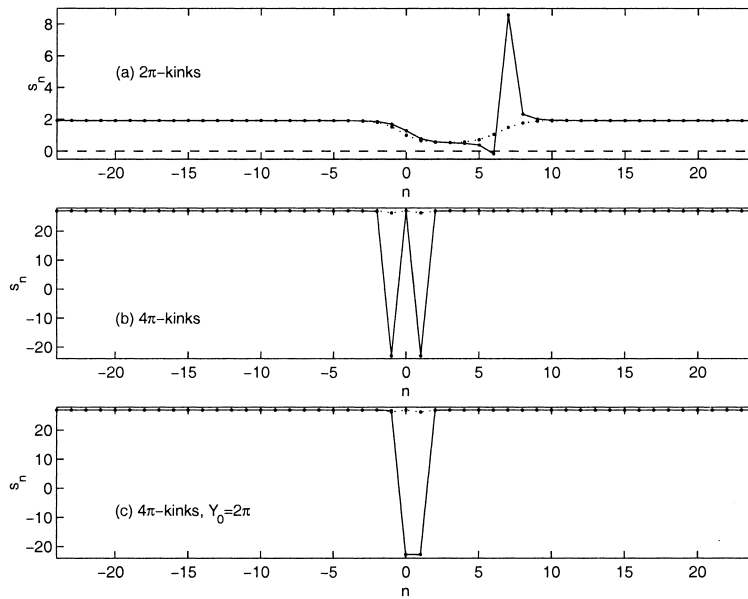


Fig. 10. Panel (a) shows the sequence s_n for 2π -kinks at $d = 1.5$ (centred kink shown by solid lines, off-centred kink by dotted lines), and panels (b) and (c) show the same for 4π -kinks at $d = 0.2$. In (b), we show the sequence for kinks with structures $(\dots, 0, \pi, 3\pi, 4\pi, \dots)$ and $(\dots, 0, 0, 4\pi, 4\pi, \dots)$ at $d = 0$; in (c), we show s_n for kinks with $(\dots, 0, \pi, 2\pi, 3\pi, 4\pi, \dots)$ and $(\dots, 0, 0, 2\pi, 4\pi, 4\pi, \dots)$ at $d = 0$.

In general $\lambda = 0$ is not an eigenvalue, so we expect $s_L = r_2$ and thus

$$\mathcal{D}(\lambda = 0) = \sqrt{1 + 4d^2} \frac{u_L}{dr_2^{L-1}}. \quad (41)$$

Hence our condition $\mathcal{D}(0) < 0$ for one unstable mode hinges on the sign of u_L .

But $u_n = s_n u_{n-1}$, and so if $s_n > 0$ for all n , then u_L is positive (we begin with $u_{-L} > 0$ in order to satisfy the normalization condition $\mathcal{D}(\lambda) \rightarrow (1, 0)$ as $|\lambda| \rightarrow \infty$). But if just one of the s_n 's is negative, then $y_L < 0$ and we violate that stability condition.

Thus, in the case of a single unstable mode, there is one sign change in the sequence s_n , and $\mathcal{D}(0) < 0$. However, if we have multiple instabilities, $\mathcal{D}(0)$ can be of either sign and we must study the structure of the Nyquist plot in more detail to detect their total number. Yet this case of multiple instabilities is unravelled much more easily with the bisection method; we need only count the number of sign changes in the sequence s_n (see Fig. 10(b) and (c)), which is also the computation needed to construct $\mathcal{D}(0)$. Thus we have a shortcut to a sufficient stability condition.

The bisection method, though being in this sense more convenient, relies on the special tridiagonal form of the stability matrix. The Evans function on the other hand is applicable to much more general systems. In any event, the methods provide systematic and powerful tools to determine stability.

One can also derive some rigorous results for stability based on the bisection method even without computing the form of the kink. These results follow on replacing the diagonal entries, A_n , with either their upper and lower bounds. Constructions of this kind allow us to show, for example, that centred 2π -kinks are unstable for $d < 0.865$. Because these kinks are actually unstable for all d we do not give details of the calculation here.

5. Conclusions

In this article we have introduced a discrete version of the Evans function technique for studying the linear eigenvalue spectrum of localized structures. In particular, for illustration, we have considered kinks in the discrete sine-Gordon system. For that system previous numerical simulations and simple arguments based on energy and the $d = 0$ limit have indicated that off-centred 2π -kinks are stable, as well as several 4π -kinks. The Evans function analysis neatly extracts these previously observed stability results, and accurately detects internal modes. Thus the Evans functions allow us to study the modifications of the eigenspectrum wrought by discreteness.

Another method for analyzing stability is via the energy stability theory often used in Hamiltonian systems [26]. This theory can also be applied in the current context, and has similarities with that of Laedke et al. [27–29], who show the stability of solitary structures in the discrete nonlinear Schrödinger equations. Unfortunately the energy stability theory offers little insight into the stability of fronts in the discrete sine-Gordon system; Evans function and bisection methods prove to be more powerful.

Another class of solutions for the sine-Gordon model where stability is not so clearly determined are *breathers*. That is, spatially localized excitations with temporal periodicity [23,30]. Intensive studies of the stability of these solutions have recently been undertaken in [31–33]. The analysis of the stability of breathers is substantially more involved than the kink stability we have described; essentially, it is an infinite-dimensional Floquet problem. However, in the rotating wave *approximation* [34–36], this stability problem simplifies significantly, and we have been able to address the problem with Evans functionology [37]. This approximation amounts to studying small amplitude breather excitations involving only a few lattice sites; importantly, we neglect all temporal harmonics of a base frequency, and so the analysis reduces to a form much like the kink stability problem. Nevertheless, the most natural way to address the general stability problem of breathers on infinite lattices is perhaps through techniques related to our Evans functions.

Because the types of bifurcations to instability are somewhat limited in the sine-Gordon model, our results are in this sense a little disappointing. However, the primary purpose for using this particular lattice is mainly one of illustration. For general systems Evans functions have important utility in categorizing the kinds of instabilities an equilibrium can suffer. This categorization is basically reflected in the geometry of the Nyquist plots. Evans functions are particularly useful in studying bifurcations to instability directly through the continuous spectrum (the examples here always occur through the origin, away from continuum). In continuous PDEs, such instabilities were analyzed with Evans functions in [12–15]. In fact, the model considered in [14] was the continuum limit of a discrete lattice.

An important distinction with the continuous problem is that Evans functions provide a general technique for analyzing the stability of localized structures whether they are moving or static. The reason why we are unable to provide a similar, general theory here, is basically the lack of translational invariance. That lack of symmetry indicates that travelling solutions rarely exist without an attendant radiation loss in the sine-Gordon model. Such structures do exist in some modified versions of discrete sine-Gordon [38,39], and in discrete Klein–Gordon and Nagumo models [6,40]. However, such systems cannot be dealt with very easily because the equations for these moving objects are, in general, differential equations with advances and delays over a lattice spacing. This makes the problem of determining the kinks themselves significantly more involved, let alone the stability analysis. A comprehensive theory of these structures is the next, very challenging step (some asymptotic theories are given in [6,8], and some related developments in simple coupled map lattices are described in [41]).

Despite this caveat, static solutions (or breathers in a rotating wave approximation) are simpler to deal with, and this is where our Evans technology can be immediately applied. In this regard, we emphasize that we need not deal with Hamiltonian systems such as the sine-Gordon model. Evans functionology works equally as well for dissipative systems. Thus one might also study the damped and driven Frenkel–Kontorova model (which is used as a model in molecular dynamics and friction), and in the coupled Lorenz model explored in [42], where stationary fronts appear. Static localized structures in coupled map lattices can also be studied with our methods. Indeed, in coupled logistic maps, kink dynamics is of notable importance [43]. Though time is now also discrete in these systems, the Evans functionology can be immediately carried over, because the eigenvalue problem is identical.

We are also not restricted to problems in one spatial dimension. The stability of structures such as planar fronts can also be determined using Evans functions [42]; the extension of the theory amounts to simply decomposing perturbations transverse to the front into Fourier components, each of which then satisfies a one-dimensional equation. One application is the stability of interfaces in the coupled map lattices studied by Kapral et al. [44].

Acknowledgements

We thank Phil Morrison, Hercules Varlamis and Michael Weinstein for useful discussions. PGK gratefully acknowledges a fellowship from the A.S. Onassis Public Benefit Foundation and an assistantship from the Computational Chemodynamics Laboratory. RVC thanks the EPSRC for providing support via an Advanced Fellowship, and NJB thanks the I.S.I. Foundation, Torino, for hospitality during part of this work.

We are grateful for the stimulating environment, and support, of the 1998 Geophysical Fluid Dynamics summer study program, Woods Hole Oceanographic Institution where this research project was initiated.

References

- [1] M. Peyrard, M.D. Kruskal, Kink dynamics in the highly discrete sine-Gordon system, *Physica D* 14 (1984) 88.
- [2] J.A. Combs, S. Yip, Single-kink dynamics in a one-dimensional atomic chain – a nonlinear atomistic theory and numerical simulation, *Phys. Rev. B* 28 (1983) 6873.

- [3] P. Stancioff, C. Willis, M. El-Batanouny, S. Burdick, Sine-Gordon kinks on a discrete lattice. 2. Static properties, *Phys. Rev. B* 33 (1986) 1912.
- [4] R. Boesch, C. Willis, M. El-Batanouny, Spontaneous emission of radiation from a discrete sine-Gordon kink, *Phys. Rev. B* 40 (1989) 2284.
- [5] R. Boesch, P. Stancioff, C.R. Willis, Hamiltonian equations for multiple-collective-variable theories of nonlinear Klein–Gordon equations – a projection-operator approach, *Phys. Rev. B* 38 (1988) 6713.
- [6] J.P. Keener, Propagation and its failure in coupled systems of discrete excitable cells, *SIAM J. Appl. Math.* 47 (1987) 556.
- [7] J.P. Keener, The effects of discrete gap junction coupling on propagation in myocardium, *J. Theor. Biol.* 148 (1991) 49.
- [8] T. Erneux, G. Nocolis, Propagating waves in discrete bistable reaction–diffusion systems, *Physica D* 67 (1993) 237.
- [9] J.P. Laplante, T. Erneux, Propagation failure in arrays of coupled bistable chemical reactors, *J. Phys. Chem.* 96 (1992) 4931.
- [10] R.S. MacKay, J.A. Sepulchre, Multistability in networks of weakly coupled bistable units, *Physica D* 82 (1995) 243.
- [11] J. Evans, Nerve axon equations, IV: the stable and unstable impulse, *Indiana Univ. Math. J.* 24 (1975) 1169.
- [12] R.L. Pego, M.I. Weinstein, Eigenvalues and instabilities of solitary waves, *Phil. Trans Roy. Soc. A* 340 (1993) 47.
- [13] R.L. Pego, P. Smereka, M.I. Weinstein, Oscillatory instability of traveling waves for a KdV–Burgers equation, *Physica D* 67 (1993) 45.
- [14] R.L. Pego, P. Smereka, M.I. Weinstein, Oscillatory instability of solitary waves in a continuum model of lattice vibrations, *Nonlinearity* 8 (1995) 921.
- [15] N.J. Balmforth, R.V. Craster, S.J.A. Malham, Unsteady fronts in an autocatalytic system, *Proc. Roy. Soc. Lond. A* 455 (1999) 1401.
- [16] J. Alexander, R. Gardner, C. Jones, A topological invariant arising in the stability analysis of travelling waves, *J. reine angew. Math.* 410 (1990) 167.
- [17] J. Frenkel, T. Kontorova, On the theory of plastic deformation and twinning, *J. Phys. USSR* 13 (1938) 137.
- [18] O.M. Braun, Y.S. Kivshar, M. Peyrard, Kink’s internal modes in the Frenkel–Kontorova model, *Phys. Rev. E* 56 (1997) 6050.
- [19] Y.S. Kivshar, D.E. Pelinovsky, T. Cretegny, M. Peyrard, Internal modes of solitary waves, *Phys. Rev. Lett.* 80 (1998) 5032.
- [20] W. Givens, Tech. Rep., Oak Ridge Natl. Lab. ORNL-1574, unpublished.
- [21] J.H. Wilkinson, *The Algebraic Eigenvalue Problem*, Clarendon Press, Oxford, 1965.
- [22] C. Baesens, S. Kim, R.S. MacKay, Localised modes on localised equilibria, *Physica D* 113 (1998) 242.
- [23] R.S. MacKay, S. Aubry, Proof of existence of breathers for time-reversible or Hamiltonian networks of weakly coupled oscillators, *Nonlinearity* 7 (1994) 1623.
- [24] S. Aubry, G. Abramovici, Chaotic trajectories in the standard map. The concept of anti-integrability, *Physica D* 43 (1990) 199.
- [25] T. Kapitula, B. Stanstedte, Stability of bright solitary-wave solutions to perturbed nonlinear Schrödinger equations, *Physica D* 124 (1998) 58.
- [26] P.J. Morrison, Hamiltonian description of the ideal fluid, *Rev. Mod. Phys.* 70 (1998) 467.
- [27] E.W. Laedke, K.H. Spatschek, S.K. Turitsyn, Stability of discrete solitons and quasicollapse to intrinsically localized modes, *Phys. Rev. Lett.* 73 (1994) 1055.
- [28] E.W. Laedke, K.H. Spatschek, S.K. Turitsyn, V.K. Mezentsev, Analytic criterion for soliton stability in a nonlinear fiber array, *Phys. Rev. E* 52 (1995) 5549.
- [29] B.W. Laedke, O. Kluth, K.H. Spatschek, Existence of solitary solutions in nonlinear chains, *Phys. Rev. B* 54 (1996) 4299.
- [30] J.L. Marin, S. Aubry, Breathers in nonlinear lattices: numerical calculation from the anticontinuous limit, *Nonlinearity* 9 (1996) 1501.
- [31] R.S. MacKay, J.A. Sepulchre, Stability of discrete breathers, *Physica D* 119 (1998) 148.
- [32] J.L. Marin, S. Aubry, Finite size effects on instabilities of discrete breathers, *Physica D* 119 (1998) 163.
- [33] S. Aubry, T. Cretegny, Mobility and reactivity of discrete breathers, *Physica D* 119 (1998) 34.
- [34] J.B. Page, Asymptotic solutions for localized vibrational modes in strongly anharmonic periodic systems, *Phys. Rev. B* 41 (1990) 7835.
- [35] A.J. Sievers, S. Takeno, Intrinsic localized modes in anharmonic crystals, *Phys. Rev. Lett.* 61 (1988) 970.
- [36] K.W. Sandusky, J.B. Page, K.E. Schmidt, Stability of motion of intrinsic localized modes in nonlinear periodic lattices, *Phys. Rev. B* 46 (1992) 6161.
- [37] P.G. Kevrekidis, in: J.-L. Thiffeault, S. Meacham (Eds.), *Geophysical Fluid Dynamics*, vol. WHOI-98, Woods Hole Oceanographic Institution, Woods Hole, MA, 1998.
- [38] J.M. Speight, R.S. Ward, Kink dynamics in a novel discrete sine-Gordon system, *Nonlinearity* 7 (1994) 475.
- [39] W.J. Zakrzewski, A modified discrete sine-Gordon model, *Nonlinearity* 8 (1995) 517.
- [40] D.B. Duncan, J.C. Eilbeck, H. Feddersen, J.A.D. Wattis, Solitons on lattices, *Physica D* 68 (1993) 1.
- [41] R. Carretero-Gonzales, D.K. Arrowsmith, F. Vivaldi, Mode-locking in coupled map lattices, *Physica D* 49 (1997) 3641.
- [42] N.J. Balmforth, C. Pasquero, A. Provenzale, The Lorenz–Fermi–Pasta–Ulam experiment, *Physica D*, (1999), submitted for publication.
- [43] Theory and applications of coupled map lattices, in: K. Kaneko (Ed.), *Nonlinear Science: Theory and Applications*, Wiley, West, UK, 1993.
- [44] R. Kapral, R. Livi, G.L. Oppo, A. Politi, Dynamics of complex interfaces, *Phys. Rev. E* 49 (1994) 2009.